nanoenergy advances

MDPI

Article

Surface Charge: An Advantage for the Piezoelectric Properties of GaN Nanowires

Tanbir Kaur Sodhi [1,2], Pascal Chrétien [2], Quang Chieu Bui [1], Amaury Chevillard [1], Laurent Travers [1], Martina Morassi [1], Maria Tchernycheva [1], Frédéric Houzé [2] and Noelle Gogneau [1,*]

[1] Centre de Nanosciences et Nanotechnologies, Université Paris-Saclay, CNRS, UMR9001, Boulevard Thomas Gobert, 91120 Palaiseau, France; tanbirkaursodhi@gmail.com (T.K.S.); quang-chieu.bui@universite-paris-saclay.fr (Q.C.B.); amaury.chevillard@c2n.upsaclay.fr (A.C.); laurent.travers@c2n.upsaclay.fr (L.T.); martina.morassi@c2n.upsaclay.fr (M.M.); maria.tchernycheva@c2n.upsaclay.fr (M.T.)

[2] Laboratoire de Génie Electrique de Paris, CNRS, CentraleSupélec, Université Paris-Saclay, 3 & 11 Rue Joliot-Curie, 91192 Gif-sur-Yvette, France; pascal.chretien@geeps.centralesupelec.fr (P.C.); frederic.houze@geeps.centralesupelec.fr (F.H.)

* Correspondence: noelle.gogneau@c2n.upsaclay.fr

Abstract: The optimization of the new generation of piezoelectric nanogenerators based on 1D nanostructures requires a fundamental understanding of the different physical mechanisms at play, especially those that become predominant at the nanoscale regime. One such phenomenon is the surface charge effect (SCE), which is very pronounced in GaN NWs with sub-100 nm diameters. With an advanced nano-characterization tool derived from AFM, the influence of SCE on the piezo generation capacity of GaN NWs is investigated by modifying their immediate environment. As-grown GaN NWs are analysed and compared to their post-treated counterparts featuring an Al_2O_3 shell. We establish that the output voltages systematically decrease by the Al_2O_3 shell. This phenomenon is directly related to the decrease of the surface trap density in the presence of Al_2O_3 and the corresponding reduction of the surface Fermi level pinning. This leads to a stronger screening of the piezoelectric charges by the free carriers. These experimental results demonstrate and confirm that the piezo-conversion capacity of GaN NWs is favoured by the presence of the surface charges.

Keywords: GaN NWs; surface charge effects; piezoelectric conversion

Citation: Sodhi, T.K.; Chrétien, P.; Bui, Q.C.; Chevillard, A.; Travers, L.; Morassi, M.; Tchernycheva, M.; Houzé, F.; Gogneau, N. Surface Charge: An Advantage for the Piezoelectric Properties of GaN Nanowires. *Nanoenergy Adv.* **2024**, *4*, 133–146. https://doi.org/10.3390/nanoenergyadv4020008

Academic Editor: Chris R. Bowen

Received: 31 July 2023
Revised: 5 March 2024
Accepted: 26 March 2024
Published: 2 April 2024

Copyright: © 2024 by the authors. Licensee MDPI, Basel, Switzerland. This article is an open access article distributed under the terms and conditions of the Creative Commons Attribution (CC BY) license (https://creativecommons.org/licenses/by/4.0/).

1. Introduction

The development of new ultracompact and highly efficient energy harvesting technologies is a key worldwide challenge, spurred by the constantly increasing use of portable smart objects both in our daily lives, as well as in high-tech applications. Among the available sources of renewable energies, mechanical deformations and vibrations originating from bodily or vehicular movements, acoustic waves, displacing fluids or friction present the advantage of being ubiquitous, available at all times and highly suitable for multiscale integration. These can be converted into an electrical output via piezoelectric systems.

In this context, nano-generators integrating piezoelectric nanowires (NWs) represent a very promising alternative compared to conventional piezo-generators based on 2D or bulk materials. In fact, thanks to their large aspect ratio and quasi-perfect crystalline quality, NWs are characterised by superior mechanical and piezoelectric properties [1–3]. In addition, NWs characterised by sub-100 nm diameters exhibit nanometre-scale phenomena, opening up new possibilities for the modulation of their properties.

The first demonstration of direct piezoelectric conversion from 1D nanostructures was evidenced with ZnO NWs [4]. Following the establishment of this new concept, other piezoelectric nanostructures have demonstrated their ability to convert a mechanical input into an electrical signal, such as PZT [5], CdS [6], CdSe [7], $BaTiO_3$ [8], $KNBO_3$ [9], GaAs [10],

Ga(In)N [11–13] and ZnO [4,14,15], the widely used semiconductor in NW-based piezo nanogenerators. Particularly, output signals up to 470 mV per nanowire [12] have been reported. Rapidly, nanogenerators integrating NWs have been demonstrated based on two main configurations: the lateral nanowire integrated nanogenerators (LINGs) and the vertical nanowire integrated nanogenerators (VINGs) [16]. While these nanogenerators can deliver output power densities reaching up to a few tens of $\mu W/cm^2$ or a few mW/cm^3 under laboratory conditions [17–24], their piezoelectric response remains very sensitive to their measurement conditions and environment. This sensitivity is due to a number of physical phenomena that become predominant in the nanoscale regime. Therefore, the enhancement of the piezoelectric coefficients [25–27], or the formation of nanocontact at the NW/electrode interface leading to an enhanced energy harvesting [28], have been demonstrated. Only a deep understanding of all the phenomena in play can allow fine control of the piezoelectric response of these nanostructures and, more largely, a suitable device performance optimization.

The purpose of this paper is to address one important phenomenon particularly pronounced in sub-100 nm wide GaN [29–32]: the surface charge effect (SCE). This effect is associated with the abrupt interruption of the atomistic structure of a material at its surfaces, where the absence of neighbouring atoms results in a different electron density as compared to the bulk. This leads to the creation of new electronic states within the semiconductor bandgap, commonly known as surface charges (SCs) [33].

The presence of these surface charges creates an energetically unfavourable situation, where charge neutrality is required to achieve stabilization at the Fermi level [33]. Consequently, a charge transfer occurs between the surface and the bulk of the material, resulting in the creation of a space charge region at the interface, commonly referred to as the depletion layer. The width of this layer is a function of the doping level of the material [34]. Thus, a built-in electric field is created at the interface, and a strong band bending occurs associated with the alignment of the surface and bulk Fermi levels (also defined as surface Fermi level pinning (SFLP)) [34–38].

Unlike bulk materials, the SFLP can partially or even fully deplete sub-100 NWs, inducing a local decrease in the diffusivity of the free charge carriers and, consequently, of their conductance [39,40]. The origin of these surface charges might vary from one system to another. In GaN NWs, they originate mainly from covalent dangling bonds [29], bistable defects [41], nitrogen anti-sites or Ga vacancies [34,42,43]. In contrast, in ZnO NWs, surface charges appear due to stabilization processes, including reconstruction, impurities and chemical adsorbates incorporation [44]. The absorption of dioxygen atoms, which act as electron acceptors, is favoured [45,46]. In GaN, Ga–O surface bonds seem to be at the origin of the strong surface trap density [45].

While the surface charges are detrimental for the optoelectronic device performance, they present an advantage for piezoelectric applications. In semiconductor materials presenting piezoelectric properties, free charge carriers are known to degrade the piezoelectric response by screening the generated piezo-charges [47–49]. This phenomenon has been evidenced in ZnO [50–52] and GaN [48] NWs. The advantageous role of the SCE is clearly illustrated in chemically synthesised ZnO NWs. In fact, these 1D nanostructures grown by hydrothermal-based synthesis methods are generally characterised by a strong intrinsic doping [53,54] sufficiently high to screen the quasi-totality of the piezo-charges. However, a non-negligible piezo-response has been reported by several groups [14,55–57]. This unexpected response results from the presence of surface traps and, thus, the resulting SFLP, limiting free carrier diffusion and leading to lower piezo-charge screening. Consequently, the internal piezoelectric field within the ZnO NWs increases, allowing for a piezoelectric response to be harvested [49].

While nanogenerators integrating NWs have been investigated for almost two decades, only a few papers have considered the crucial role of the SCE. The first exploration of this effect dates back to 2018, with theoretical simulations reported by Tao et al. [49]. In this study, the piezo-potential variation in the NWs was simulated as a function of the charge

carrier concentration, NW morphology and pinning conditions. Considering the SFLP, an increase in the NW's piezo-potential by a factor of 10 to 16 times was observed as compared to NWs without SFLP. More recently, the relationship between the surface charge effect and the piezoelectric response of the NWs as a function of their diameter has been demonstrated. In ZnO NWs, the group of G. Ardila [57] observed variations in the piezoelectric coefficient d_{33} as a function of the NW diameter. In GaN NWs, our group has demonstrated the enhancement of the piezoelectric coupling coefficient from 5% to 43% by taking advantage of the surface charges, with pronounced effects for a specific NW diameter window [58]. In both these cases, the enhancement of the piezoelectric response is linked to the decrease in NW diameter, leading to its depletion and limiting the diffusion of surface-free carriers within the material, thus mitigating their screening impact.

Surface charges and trap densities have been reported to be of the order of 10^{12}–10^{13} cm^{-2}, as determined though electrical and optical characterization techniques [30–32]. These characteristics are inherent to the material itself and the nanostructure growth mode [40]. Notably, they exhibit strong sensitivity to the nanostructure environment. Consequently, a limited number of research groups have undertaken the functionalization of nanostructures to modulate the piezoelectric responses of the nanogenerators. Strategies such as gas adsorption or nanoparticles deposition onto the NW surface have been employed for this purpose, as demonstrated by X. Xue et al. [47] and S. Lu et al. [59]. These approaches aim to modulate the depletion width within the NWs, thereby reducing the effective screening.

In the present study, we investigate the influence of SCE on the piezo generation capacity of GaN NWs by modifying their immediate environment. Both as-grown GaN NWs and post-treated NWs with an atomic layer deposition treatment to form an Al_2O_3 shell surrounding the GaN NW core are considered. To ensure that the expression of the surface charge is solely influenced by the NW environment, the investigated GaN NWs maintain an approximately constant diameter. To assess the impact of the surface charges on the piezoelectric response, an advanced nano-characterization tool derived from atomic force microscopy (AFM) in employed.

Based on experimental measurements, we highlight that, for an equivalent deformation rate, the average output voltages are consistently lower for GaN/Al_2O_3 core–shell NWs compared to bare GaN NWs. This observed behaviour aligns with the reduction in the surface trap density in presence of the Al_2O_3 shell. As the surface Fermi level pinning decreases with a lower the trap density, the depletion of the NWs becomes less pronounced. Consequently, the screening of the piezo charges by the free carriers increases, resulting in a reduced output voltage. These results experimentally demonstrate and confirm that the piezo-conversion capacity of GaN NWs is favoured by the presence of surface charges.

2. Materials and Methods

Self-assembled GaN NWs were grown on a conductive Si(111) substrate (resistivity of about 0.007 Ω·cm) with a Plasma-Assisted Molecular Beam Epitaxy (PA-MBE) reactor equipped with a radio frequency N plasma source. Prior to the growth, the Si substrate was chemically cleaned and subsequently heated *in situ* at 850 °C to remove the organic pollutants and the native oxide, respectively. Then, a 2.5 nm thick AlN buffer layer was deposited at 620 °C on the clean Si surface, as describe in [60]. The objective of this AlN buffer is to control the NW nucleation and density [61,62], reduce the NW twist [63], improve the NW verticality [64] and to ensure the conductivity between the GaN NWs and the conductive Si substrate [65]. Indeed, the deposition of the AlN buffer layer involves two distinct steps. Firstly, the deoxidised Si(111) substrate is exposed at 620 °C to an Al flux, resulting in the formation of Al droplets dispersed on the surface in the form of an Al–Si eutectic [66]. Subsequently, the surface is exclusively exposed to a nitrogen flux (by switching the Al/N shutters), leading to the formation of the AlN buffer layer over the surface due to the Al diffusion. During the nitridation phase, the Si atoms dissolved into the Al droplets are incorporated into the AlN layer, causing n-doping and thereby imparting a conductive behaviour to the buffer layer. Finally, GaN NWs are grown at 770 °C under

nominally N-rich conditions (V/III = 1.36). During the growth, the Mg cell is maintained at 400 °C with a closed shutter to induce a p-type residual doping of the GaN NWs.

Under these growth conditions, vertically oriented GaN NWs crystallise in the wurtzite structure and present a hexagonal cross-section delimited by {10-10} planes [63]. Figure 1a illustrates the GaN NW morphology, characterised by a density of 3.4×10^9 NW/cm^2 and a diameter of 36 nm $\pm$ 9 nm. This approximatively constant diameter ensures that the expression of the surface charges will not be dominated by diameter effects. Regarding the NW height, a trimodal dispersion is measured, resulting in three different NW aspect ratios, as we can see in Figure 1b. This distribution in terms of the aspect ratio allows spanning a significant range of deformation rates under the same mechanical external input. Thus, it provides the opportunity to experimentally establish the intrinsic relationship between the piezo generated output voltage (OV) and the expression of the surface charges as a function of the NW surrounding environment.

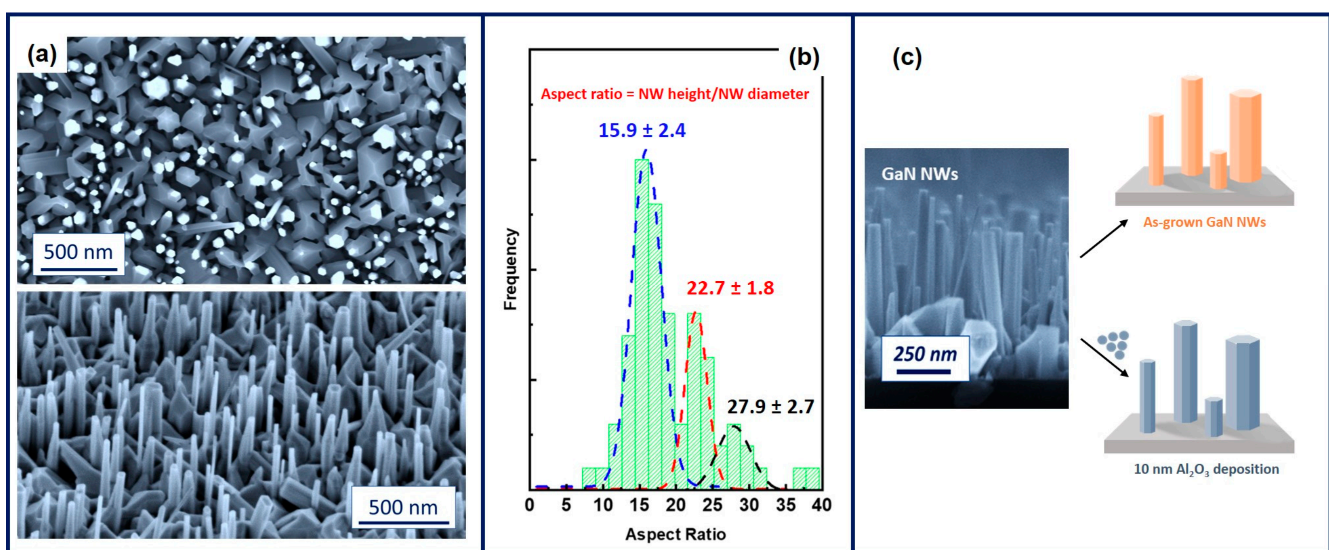

Figure 1. (**a**) Top view and titled view SEM images of as-grown GaN NWs. (**b**) Histogram representing the aspect ratio (NW height/NW diameter) population of the as-grown GaN NWs. (**c**) The same as-grown GaN NW sample has been divided into two pieces: GaN and GaN/Al_2O_3 core–shell NWs for demonstrating the influence of the surface charge effect on the piezoelectric response of the nanostructures.

To highlight the significance of the surface charge modulation as a function of the NW environment on the OV generation capacity, two portions of the same GaN NWs sample were prepared following different procedures, schematised in Figure 1c. The GaN NWs of the first portion were left unaltered, while those of the second portion were encapsulated by a 10 nm thick Al_2O_3 shell through an atomic layer deposition treatment. The Al_2O_3 shell is recognised for its ability to reduce the SCE [67–69]. In presence of the Al_2O_3 shell, the GaN NW surfaces are passivated [70–73] through a limitation or even a suppression of the Ga–O bonds [45]. As a consequence, the surface trap density is reduced by one to two orders of magnitude, resulting in a density of about 10^{11}–10^{12} cm^{-2} for GaN/Al_2O_3 core–shell NWs, while this density is about 10^{13} cm^{-2} for as-grown GaN NWs [32].

The piezoelectric responses of the NWs were quantified using an atomic force microscope (AFM) operating in contact mode, equipped with a homemade modified Resiscope module [74] designed to measure the direct piezoelectric effect in the NWs [11]. In this experimental configuration, schematised in Figure 2a, the electrical module is connected to the substrate (forming an Ohmic contact with the GaN NWs [66]) and to the Cr/Pt AFM tip (with a work function around 5.2 eV), forming a Schottky barrier with the GaN NWs (electron affinity of the GaN is about 4.1 eV [75]), ensuring the harvesting of the piezo

generated charges [50]. No external voltage is applied, and the generated electrical signals are observed across a load resistance R_L of 1 GΩ.

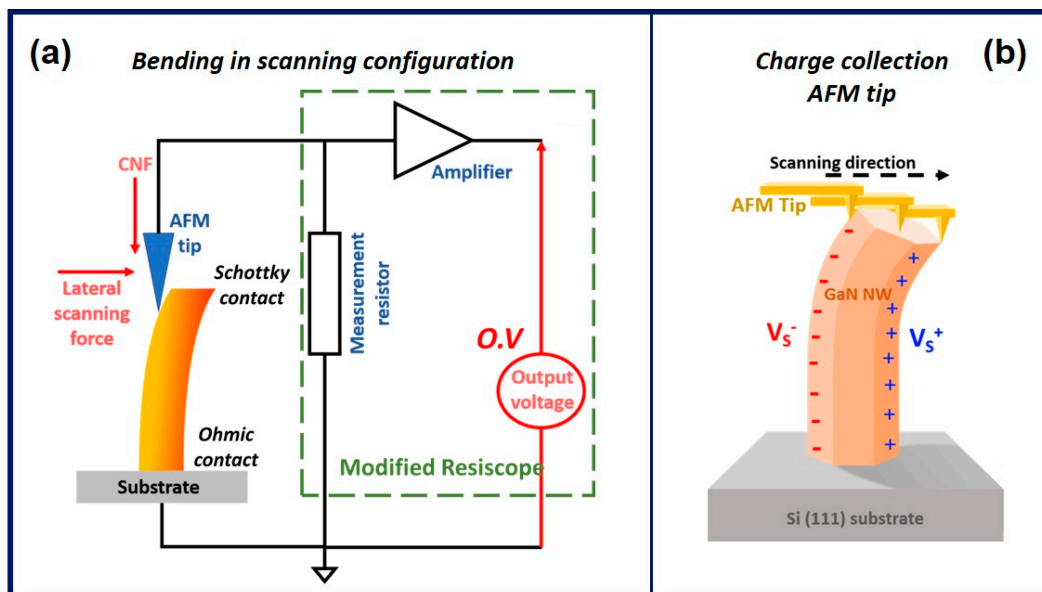

Figure 2. (**a**) Principle of the piezoelectric measurements performed by AFM equipped with a home-made modified Resiscope in the bending scanning configuration. (**b**) Distribution of the piezoelectric field in a N-polar GaN NW deformed by bending from the stretched side to the compressed one.

The piezoelectric measurements on the GaN NWs were conducted under bending deformation. The conductive AFM tip is brought in contact with the surface and scans over the GaN NW array. The force applied by the tip, resulting from the convolution of the constant normal force (CNF) and the scanning force, induces a lateral bending of the NWs. In response to its elastic deformation, and owing to its piezoelectric properties, the NW generates an output voltage harvested through the Schottky diode (Figure 2a).

For N-polar GaN NWs under bending deformation, the piezoelectric potential is distributed from a negative value on the stretch side to a positive value on the compressed side [76]. Depending on the majority charge carriers, the Schottky diode will be positively biased according to the NW doping: for n-doped GaN NWs, negative OVs are harvested when the conductive AFM tip is in contact with the negative piezo-potential, while for p-doped GaN NWs (as in the present study), positive OVs are harvested when the AFM tip is in contact with the positive piezo-potential (Figure 2b).

This modified Resiscope AFM technique combines the nanometre scale spatial resolution with real-time electrical measurements while scanning over large surfaces (several μm^2). Hence, it allows for the simultaneous recording of topographic and electrical signals. Thus, for each NW constituting the array, a direct correlation between its morphology and its electromechanical response can be established.

To perform reliable electrical measurements, and knowing that MBE-grown GaN NWs are very flexible [11], their bases were embedded into a soft polymer matrix (Figure 3a). PDMS was chosen at this scope due to its Young's modulus of about 0.9 MPa [77], which is lower than the one of the GaN NWs estimated at 1.8 GPa. This ensures mechanical consolidation of the nanostructures (preventing their fold up towards the neighbouring NWs or the substrate, leading to the leakage of the piezoelectric charges) while avoiding any strain effect on the NWs. The PDMS matrix was spin-coated and etched back by RIE using a O_2/CF_4 plasma treatment to uncover the top portion of both sets of NWs. In the specific case of GaN/Al_2O_3 core–shell NWs, two additional steps have been implemented in order to guaranty sample comparison. Before the matrix deposition, the GaN/Al_2O_3 core–shell NWs were exposed to oxygen plasma to enhance the wettability of PDMS with

the NW sidewalls and thus achieve a matrix distribution equivalent to that around the NWs. It is worth noting that this plasma treatment does not affect the surface trap density, since it is controlled by the GaN/Al_2O_3 interface. Finally, the Al_2O_3 capping the top facet of the NWs is removed by ion beam etching (IBE) to ensure the same GaN–Cr/Pt Schottky diode formed between the conductive AFM tip and the NWs.

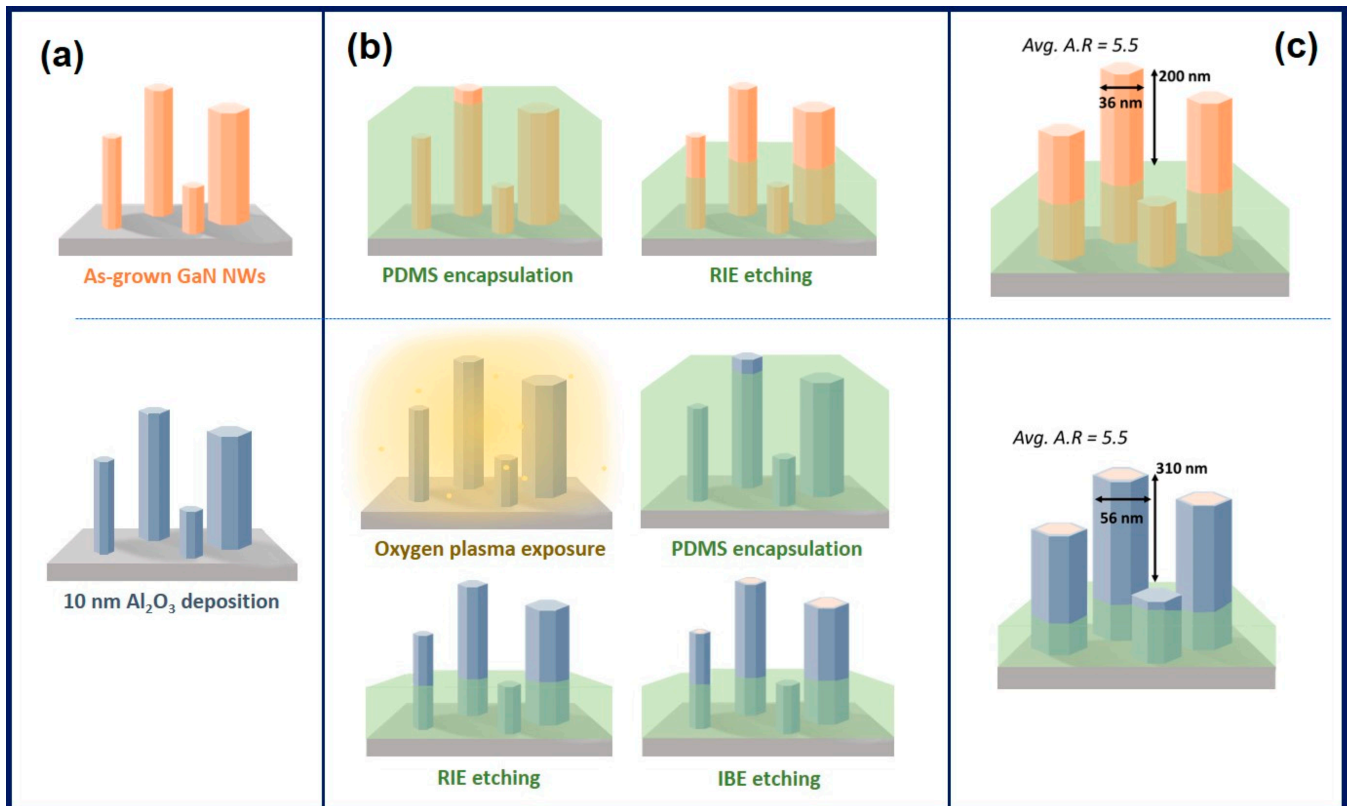

Figure 3. Schematic representation of the NW preparation. (**a**) The as-grown NW sample was divided into two portions to obtain GaN and GaN/Al_2O_3 core–shell NWs, respectively. (**b**) Nanostructures are mechanically consolidated by embedding their bases into a soft PDMS matrix. (**c**) The top portion of the consolidated NWs presents the same aspect ratio to ensure the equivalent deformation rate under applied force.

It should be noted that the deposition of the Al_2O_3 shell increases the effective diameter of the NWs, which, in return, makes them stiffer. For the sake of comparing the piezoelectric responses of the NWs with the Al_2O_3 shell and as-grown NWs, an adjustment to the NW height emanating from the PDMS matrix was made. Thus, to probe the same deformation degree under an equivalent deformation force, the average aspect ratio of the NW emerging portion has been kept constant and equal to 5.5. This aspect ratio has been chosen to be able to access multiple degrees of deformation as a function of the applied force. Thus, for GaN NWs characterised by an average diameter of 36 $\pm$ 9 nm, the average NW top portion height has been fixed at 200 nm, while, for GaN/Al_2O_3 core–shell NWs with an average diameter of 56 $\pm$ 9 nm, the NW top portion height has been fixed at 310 nm (Figure 3b).

3. Results and Discussions

In the first instance, the piezoelectric response of the 1D nanostructures depends on their deformation degree. However, the response is also affected by surface charge effects. For both sets of NWs, the topographic and output voltage mappings were simultaneously registered at constant normal forces (CNFs) ranging between 120 nN and 380 nN. The 3D electrical mappings are presented in Figure 4, and the corresponding statistical analyses are summarised in Table S1 (Supplementary Materials).

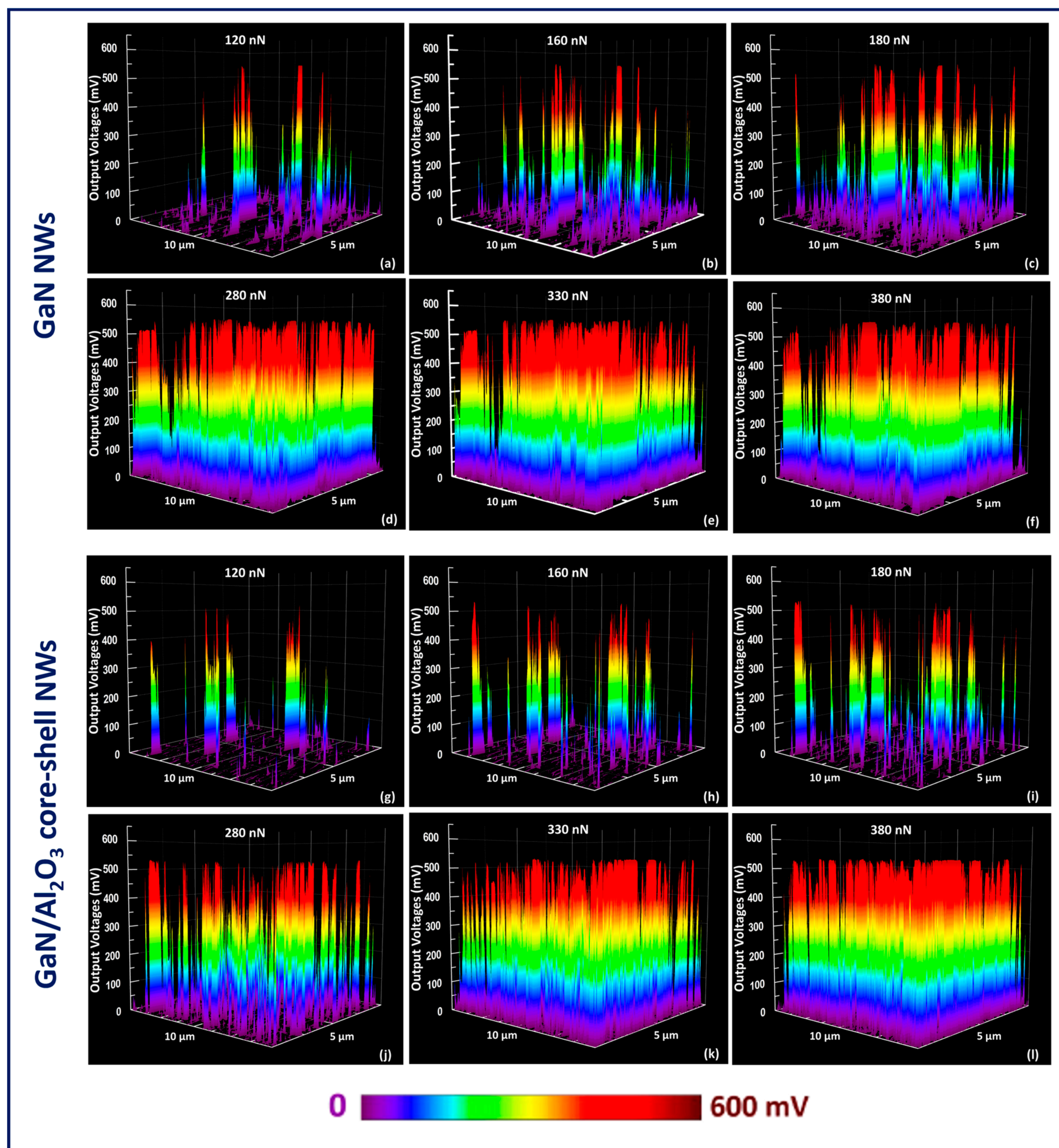

Figure 4. Three-dimensional (10 µm × 5 µm) mappings of the OVs generated by GaN NWs (**a**–**f**) and GaN/Al_2O_3 core–shell NWs (**g**–**l**) under bending deformation. The increase in the OVs with the applied constant normal force is a direct demonstration of the direct piezoelectric effect taking place.

The average output voltages are plotted as a function of the applied force in Figure 5a,b for both samples. Similar behaviours can be observed. Firstly, positive output voltages are generated by the NWs independently from their stiffness and the applied CNF. This behaviour results from the intrinsic p-type doping of the GaN NWs achieved with our growth conditions [13,24]. Secondly, the average output voltages follow Gaussian multimodal distributions, as shown in Figure 5c. This behaviour stems from the NW self-assembled growth paradigm, leading to a dispersion of morphologies [12,58]: while the NW diameter is constant, the nanostructures are characterised by a multimodal dispersion of heights and, hence, of stiffnesses. In the present case, the first distribution corresponds to the shorter and most rigid set of NWs, while the second and third distributions refer to taller and

more flexible NWs. Finally, we observe that the three distributions show an increase in the average OV when increasing the applied CNF due to the direct piezoelectric effect and the increased stability of the Schottky contact [28,78].

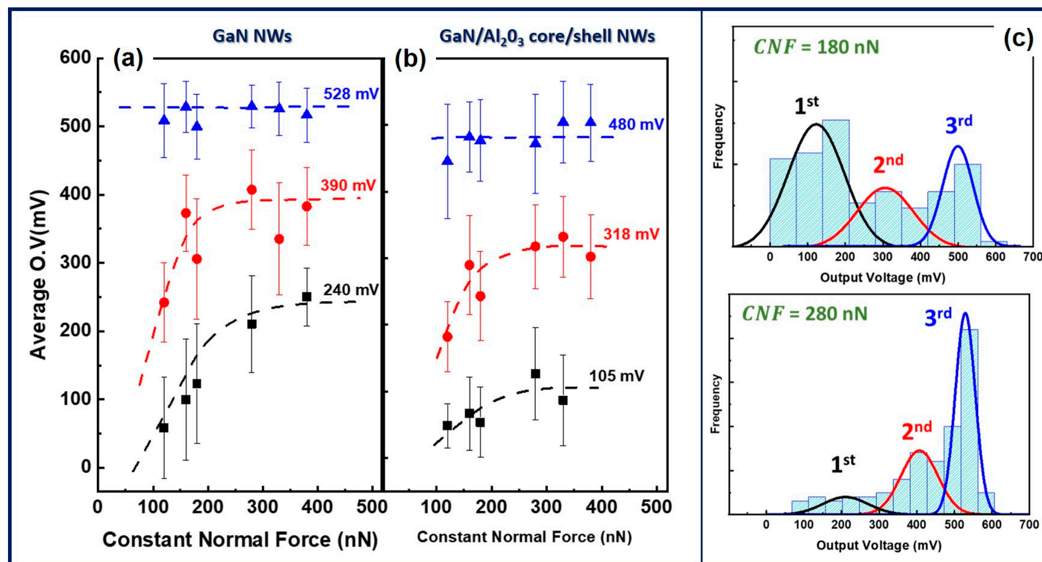

Figure 5. Statistical analysis of 3D electrical mappings for an applied force evolving in the 120–380 nN range for pure GaN NWs (**a**) and GaN/Al_2O_3 core–shell NWs (**b**). The saturation values of the different distributions are indicated for comparison. A trimodal distribution of the averaged OV is evidenced, as it is clearly visible in (**c**), showing examples of the OV distribution for two CNFs well described by Gaussian functions.

The OV variations are analysed for both sets of investigated samples. For the pure GaN NWs, the first distribution increases continuously with the applied CNF from ~58 $\pm$ 75 mV to ~250 $\pm$ 42 mV, while the second one saturates around 350 $\pm$ 62 mV for CNF $\geq$ 160 nN. The third distribution is characterised by approximatively constant OV values around 515 $\pm$ 25 mV in the whole CNF range. This means that these NWs are very flexible and attained their maxima of piezo-conversion at smaller forces. Concerning the GaN/Al_2O_3 core–shell NWs, equivalent behaviours are observed. While the first distribution increases from 49 $\pm$ 33 mV to about 100 $\pm$ 70 mV, the second one achieves a saturation around 320 $\pm$ 60 mV for CNF $\geq$ 160 nN. Finally, the third distribution is characterised by approximatively constant OV values around 480 $\pm$ 60 mV.

At this stage, it is noteworthy that GaN NWs deliver average output voltages reaching up to 528 mV per NW, marking the highest recorded OV reported in the literature for this system, to the best of our knowledge. This piezoelectric response is higher than those generated by other piezoelectric 1D nanostructures, particularly ZnO NWs, which remain the most extensively investigated nanostructures for the development of a new generation of piezoelectric energy harvesters.

We now compare the OV generated by each set of samples. As a reminder, this comparison is possible, since the average aspect ratio of the emerging NW top portion has been maintained constant (AR = 5.5) for both samples. Consequently, the NWs present equivalent deformation rates under the same AFM scanning conditions. Referring to Figures 4 and 5, along with Table S1 (Supplementary Materials), it is observed that, regardless of the applied CNF value and the specific NW distribution, the OVs generated by the GaN/Al_2O_3 core–shell NWs are systematically lower than the ones generated by the pure GaN NWs with reduction ranges from several tens of mV, representing a decrease ranging from 9 to 56%, depending on the specific NW considered.

To elucidate the variations in OVs observed among the sets of NWs, it is important to consider the different parameters influencing the NW ability to convert mechanical deformation into a direct electrical signal.

- The piezo-conversion firstly depends on the deformation degree of the material.

According to the direct piezoelectric effect, as the deformation increases, the output signal rises accordingly. Consequently, under an equivalent mechanical input, two NWs presenting a different stiffness (directly related to the NW aspect ratio) will generate distinct internal piezoelectric fields and thus different output voltages. This mechanism is schematised in Figure 6.

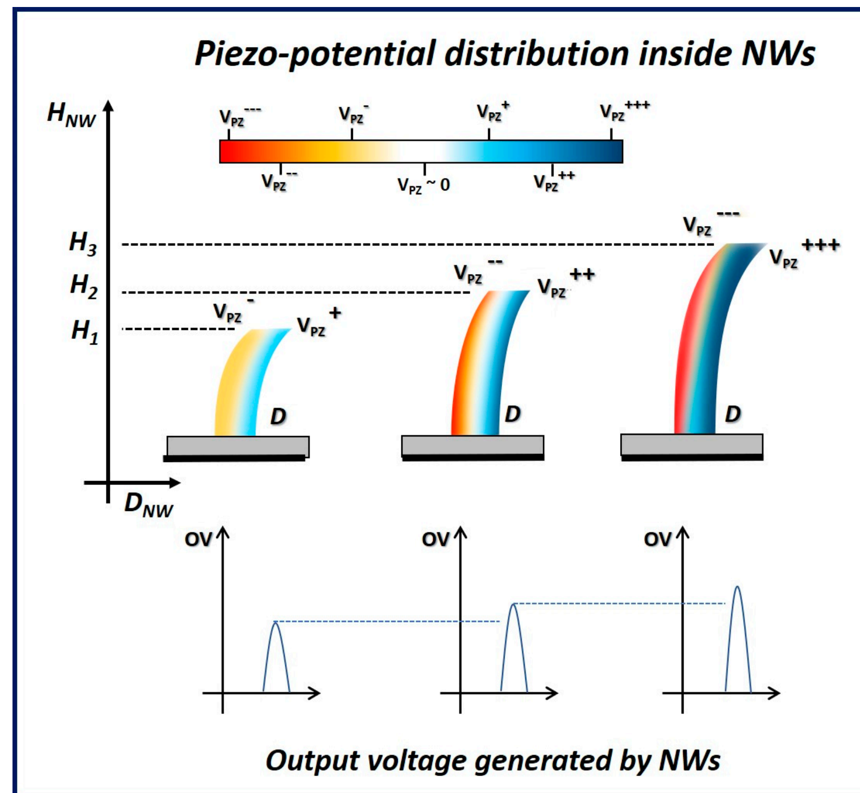

Figure 6. Schematic representation of the piezoelectric field distribution inside the NWs characterised by an equivalent diameter (D) but three different heights (H), resulting in three different aspect ratios, and the corresponding output voltage generated in response to an equivalent lateral force applied to the AFM tip. In the present experiments, the NWs being intrinsically p-doped, the OV is collected through the Schottky diode when the conductive AFM tip is in contact with the compressive NW side, where the piezo potential is positive [76].

- The piezo-conversion is directly related to the conductivity/resistivity of the NWs.

It is widely acknowledged that the free charge carriers play a crucial role in screening the generated piezo-charges, leading to a reduction in the internal piezoelectric field within the NW and consequent degradation of the output signal. As previously explained, the surface charges lead to a Fermi-level pinning in the depletion region along the NW sidewall surface formed by the M-plane facets. The extent of depletion, whether partial or complete, is contingent upon its diameter and the material's doping level [39,58]. The surface barrier height, $\Phi_B^{Surface}$, is of the order of the SFLP. For large NWs (NW diameters > two times the depletion width), a conduction channel exists surrounded by a SFLP at the NW surface (Figure 7a). In contrast, for thin NWs (NW diameters $\leq$ two times the depletion width), the NW is fully depleted (Figure 7b).

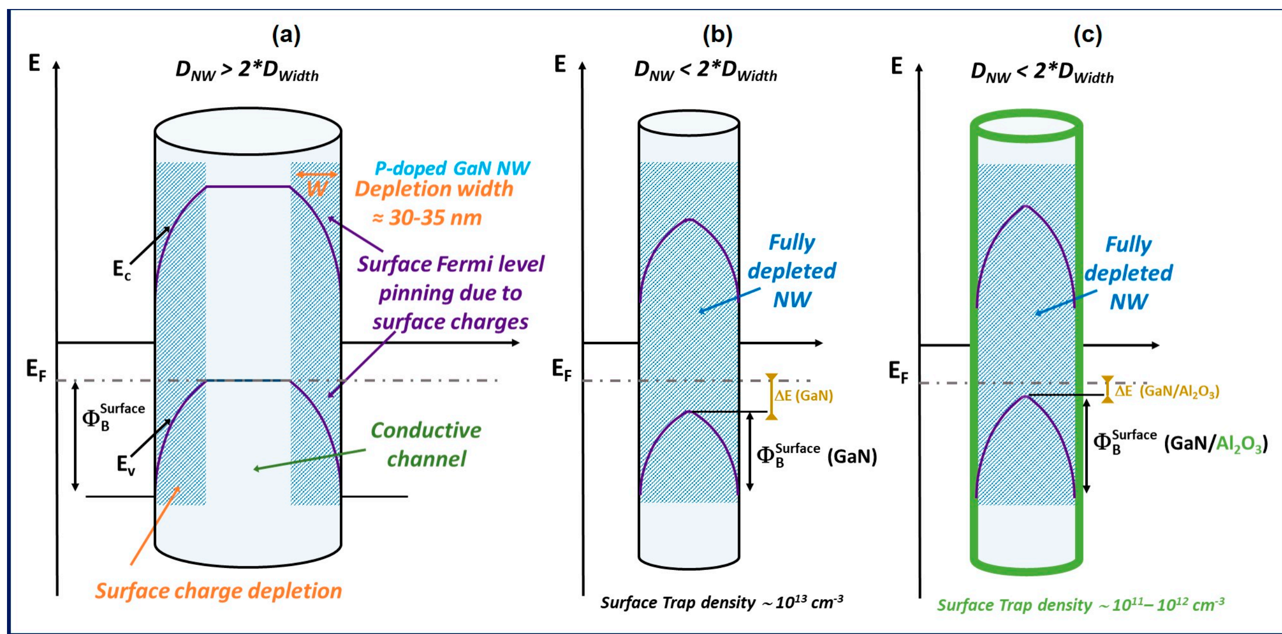

Figure 7. Schematic representation of the Fermi level pinning in p-doped NWs for (**a**) partially depleted GaN NWs. (**b**) Fully depleted GaN NWs. (**c**) Fully depleted GaN/Al_2O_3 core–shell NWs. $\Phi_B^{Surface}$ is the maximal surface barrier height, and ΔE is the energy difference between the Fermi level and the valence band maximum. For the fully depleted NWs, the $\Phi_B^{Surface}(GaN/Al_2O_3)$ is higher than the $\Phi_B^{Surface}(GaN)$, and by consequence, the ΔE(GaN/Al_2O_3) is smaller than the ΔE(GaN), due to the passivation of the GaN core by the Al_2O_3 shell inducing the reduction of the surface trap density.

Depending on the depletion degree, the band curvature and the corresponding barrier for surface electron–hole pair recombination are modulated. In other terms, a lower $\Phi_B^{Surface}$ results in a higher NW depletion and an increased difference between the Fermi level and the top of the valence band, denoted as ΔE. Consequently, the internal piezo-potential created in response to deformation will be more or less screened, leading to a corresponding decrease or increase in the generated OV.

In our intrinsically p-doped GaN NWs (doping level estimated to be around 5×10^{16} cm^{-3} from SIMS measurements on 2D GaN films), the depletion width has been estimated to be less than 30 nm [58]. With a diameter of 36 ± 9 nm, the investigated nanostructures are thus fully depleted, with the SFLP taking place across the entire NWs. Considering the OVs collected for these nanostructures (Figures 4 and 5) and an estimated surface trap density of around 10^{13} cm^{-2} for the pure GaN NWs [32], we infer a reduced band curvature. This results in a smaller barrier, noted as $\Phi_B^{Surface}(GaN)$, and thus to a non-negligible ΔE, as illustrated in Figure 7b. This configuration is thus favourable for minimising the screening of the piezoelectric charges and for enhancing the internal piezo-potential and the generated Ovs.

In the case of the same GaN NWs surrounded by the Al_2O_3 shell, the nanostructures are also considered fully depleted, since their core is defined by an unchanged doping level and diameter. However, due to their surface passivation, the surface trap density is reduced to around 10^{11}–10^{12} cm^{-2}, according to the literature [67–69]. The OVs generated by these core–shell NWs are still significant but remain systematically lower than the ones generated by the pure GaN NWs. This combination of factors indicates that, for the GaN/Al_2O_3 core–shell NWs, the SFLP is less pronounced. The surface barrier $\left(\Phi_B^{Surface}(GaN/Al_2O_3)\right)$ and the corresponding ΔE(GaN/Al_2O_3) are, respectively, higher and smaller than the ones of the GaN NWs $\left(\Phi_B^{Surface}(GaN), \Delta E(GaN)\right)$, as illustrated in Figure 7c. As a consequence,

for an equivalent deformation degree, the screening of the piezo-charges is higher, leading to a reduction of the piezoelectric field and resulting OVs.

These experimental measurements thus demonstrate that the surface charge effect is favourable for enhancing the piezoelectric conversion efficiency in 1D-nanostructures.

4. Conclusions

While the piezoelectric response of materials is preliminarily regulated by the deformation rate, the role of the surface charges cannot be overlooked, especially in sub-100 nm wide NWs. The results presented in this study experimentally demonstrate that surface charges can play a favourable role by increasing the piezo-generation capacity of non-intentionally p-type doped GaN NWs. Consequently, by modifying the NW environment, it is possible to modulate the piezoelectric response of GaN NWs, known for their surface trap density on the order of 10^{13} cm^{-2}. The passivation of the GaN core by an Al_2O_3 shell leads to a noticeable reduction in the surface charge density, resulting in a significant decrease of the output voltages due to reduced surface Fermi level pinning and the resulting enhanced screening of the internal piezoelectric field. To support this conclusion, further investigations involving different shells and the quantification of the surface trap density are currently underway.

Leveraging the surface charge effect, the OVs generated by GaN NWs can reach an average value of 529 mV. This outcome stands as the highest reported in the literature for GaN NWs and exceeds the ones reported other piezoelectric 1D nanostructures.

In conclusion, surface engineering for the modulation and control of surface trap densities opens up new pathways to enhance the piezoelectric conversion efficiency of NWs and thus improve the performance of devices integrating these 1D nanostructures.

Supplementary Materials: The following supplementary materials can be downloaded at https://www.mdpi.com/article/10.3390/nanoenergyadv4020008/s1: Table S1: Statistical analyses of the output voltage mappings registered at constant normal forces (CNFs) ranging between 120 nN and 380 nN for the three aspect ratio distributions.

Author Contributions: T.K.S.: conceptualisation, formal analysis, investigation and writing—original draft preparation; P.C.: conceptualisation, validation, formal analysis, investigation and supervision; Q.C.B.: formal analysis and technical support; A.C.: formal analysis and technical support; L.T.: technical support; M.M.: writing—original draft preparation; M.T.: project administration and funding acquisition; F.H.: validation, formal analysis and writing—original draft preparation; N.G.: conceptualisation, validation, formal analysis, writing—original draft preparation, supervision, project administration and funding acquisition. All authors have read and agreed to the published version of the manuscript.

Funding: This work was financially supported by the French National Research Agency through the GANEX program (ANR-11-LABX-0014), the Project SCENIC (ANR-20-CE09-0005) and as part of the "Investissements d'Avenir" program (reference: ANR-10-LABX-0035, Labex NanoSaclay). Finally, this work was done within the C2N micro-nanotechnologies platforms and partly supported by the RENATECH network and the General Council of Essonn.

Data Availability Statement: Data may be made available on request and argumentation. Please contact the corresponding author.

Acknowledgments: The authors thank the administrative and technical support of both laboratories for their fruitful help.

Conflicts of Interest: There are no conflicts to declare.

References

1. Yang, P.; Yan, R.; Fardy, M. Semiconductor Nanowire: What's Next? *Nano Lett.* **2010**, *10*, 1529–1536. [CrossRef] [PubMed]
2. Qi, Y.; McAlpine, M.C. Nanotechnology-Enabled Flexible and Biocompatible Energy Harvesting. *Energy Environ. Sci.* **2010**, *3*, 1275–1285. [CrossRef]
3. Chang, C.; Tran, V.H.; Wang, J.; Fuh, Y.-K.; Lin, L. Direct-Write Piezoelectric Polymeric Nanogenerator with High Energy Conversion Efficiency. *Nano Lett.* **2010**, *10*, 726–731. [CrossRef] [PubMed]

4. Wang, Z.L.; Song, J. Piezoelectric Nanogenerators Based on Zinc Oxide Nanowire Arrays. *Science* **2006**, *312*, 242–246. [CrossRef] [PubMed]
5. Chen, C.-Y.; Liu, T.-H.; Zhou, Y.; Zhang, Y.; Chueh, Y.-L.; Chu, Y.-H.; He, J.-H.; Wang, Z.L. Electricity Generation Based on Vertically Aligned PbZr0.2Ti0.8O3 Nanowire Arrays. *Nano Energy* **2012**, *1*, 424–428. [CrossRef]
6. Lin, Y.-F.; Song, J.; Ding, Y.; Lu, S.-Y.; Wang, Z.L. Piezoelectric Nanogenerator Using CdS Nanowires. *Appl. Phys. Lett.* **2008**, *92*, 022105. [CrossRef]
7. Zhou, Y.S.; Wang, K.; Han, W.; Rai, S.C.; Zhang, Y.; Ding, Y.; Pan, C.; Zhang, F.; Zhou, W.; Wang, Z.L. Vertically Aligned CdSe Nanowire Arrays for Energy Harvesting and Piezotronic Devices. *ACS Nano* **2012**, *6*, 6478–6482. [CrossRef] [PubMed]
8. Wang, Z.; Hu, J.; Suryavanshi, A.P.; Yum, K.; Yu, M.-F. Voltage Generation from Individual BaTiO3 Nanowires under Periodic Tensile Mechanical Load. *Nano Lett.* **2007**, *7*, 2966–2969. [CrossRef] [PubMed]
9. Kang, P.G.; Lee, T.K.; Ahn, C.W.; Kim, I.W.; Lee, H.H.; Choi, S.B.; Sung, K.D.; Jung, J.H. Vertically Aligned Epitaxial KNbO3 Nanorod Array for Piezoelectric Energy Harvester and Second Harmonic Generator. *Nano Energy* **2015**, *17*, 261–268. [CrossRef]
10. Alekseev, P.A.; Sharov, V.A.; Geydt, P.; Dunaevskiy, M.S.; Lysak, V.V.; Cirlin, G.E.; Reznik, R.R.; Khrebtov, A.I.; Soshnikov, I.P.; Lähderanta, E. Piezoelectric Current Generation in Wurtzite GaAs Nanowires. *Phys. Status Solidi Rapid Res. Lett.* **2018**, *12*, 1700358. [CrossRef]
11. Gogneau, N.; Chrétien, P.; Galopin, E.; Guilet, S.; Travers, L.; Harmand, J.-C.; Houzé, F. GaN Nanowires for Piezoelectric Generators. *Phys. Status Solidi Rapid Res. Lett.* **2014**, *8*, 414–419. [CrossRef]
12. Jegenyes, N.; Morassi, M.; Chrétien, P.; Travers, L.; Lu, L.; Julien, F.; Tchernycheva, M.; Houzé, F.; Gogneau, N. High Piezoelectric Conversion Properties of Axial InGaN/GaN Nanowires. *Nanomaterials* **2018**, *8*, 367. [CrossRef] [PubMed]
13. Gogneau, N.; Jamond, N.; Chrétien, P.; Houzé, F.; Lefeuvre, E.; Tchernycheva, M. From Single III-Nitride Nanowires to Piezoelectric Generators: New Route for Powering Nomad Electronics. *Semicond. Sci. Technol.* **2016**, *31*, 103002. [CrossRef]
14. Gao, P.X.; Song, J.; Liu, J.; Wang, Z.L. Nanowire Piezoelectric Nanogenerators on Plastic Substrates as Flexible Power Sources for Nanodevices. *Adv. Mater.* **2007**, *19*, 67–72. [CrossRef]
15. Lu, M.-P.; Song, J.; Lu, M.-Y.; Chen, M.-T.; Gao, Y.; Chen, L.-J.; Wang, Z.L. Piezoelectric Nanogenerator Using P-Type ZnO Nanowire Arrays. *Nano Lett.* **2009**, *9*, 1223–1227. [CrossRef]
16. Pawar, O.Y.; Patil, S.L.; Redekar, R.S.; Patil, S.B.; Lim, S.; Tarwal, N.L. Strategic Development of Piezoelectric Nanogenerator and Biomedical Applications. *Appl. Sci.* **2023**, *13*, 2891. [CrossRef]
17. Lu, L.; Jamond, N.; Chrétien, P.; Houzé, F.; Travers, L.; Harmand, J.C.; Glas, F.; Julien, F.H.; Lefeuvre, E.; Gogneau, N.; et al. Nitride Nanowires: From Rigid to Flexible Piezo-Generators. *J. Phys. Conf. Ser.* **2016**, *773*, 012010. [CrossRef]
18. Waseem, A.; Johar, M.A.; Hassan, M.A.; Bagal, I.V.; Abdullah, A.; Ha, J.-S.; Lee, J.K.; Ryu, S.-W. Flexible Self-Powered Piezoelectric Pressure Sensor Based on GaN/p-GaN Coaxial Nanowires. *J. Alloys Compd.* **2021**, *872*, 159661. [CrossRef]
19. Johar, M.A.; Waseem, A.; Hassan, M.A.; Bagal, I.V.; Abdullah, A.; Ha, J.; Ryu, S. Highly Durable Piezoelectric Nanogenerator by Heteroepitaxy of GaN Nanowires on Cu Foil for Enhanced Output Using Ambient Actuation Sources. *Adv. Energy Mater.* **2020**, *10*, 2002608. [CrossRef]
20. Ye, S.; Cheng, C.; Chen, X.; Chen, X.; Shao, J.; Zhang, J.; Hu, H.; Tian, H.; Li, X.; Ma, L.; et al. High-Performance Piezoelectric Nanogenerator Based on Microstructured P(VDF-TrFE)/BNNTs Composite for Energy Harvesting and Radiation Protection in Space. *Nano Energy* **2019**, *60*, 701–714. [CrossRef]
21. Cha, S.; Kim, S.M.; Kim, H.; Ku, J.; Sohn, J.I.; Park, Y.J.; Song, B.G.; Jung, M.H.; Lee, E.K.; Choi, B.L.; et al. Porous PVDF As Effective Sonic Wave Driven Nanogenerators. *Nano Lett.* **2011**, *11*, 5142–5147. [CrossRef] [PubMed]
22. Zhu, G.; Wang, A.C.; Liu, Y.; Zhou, Y.; Wang, Z.L. Functional Electrical Stimulation by Nanogenerator with 58 V Output Voltage. *Nano Lett.* **2012**, *12*, 3086–3090. [CrossRef] [PubMed]
23. Dahiya, A.S.; Morini, F.; Boubenia, S.; Justeau, C.; Nadaud, K.; Rajeev, K.P.; Alquier, D.; Poulin-Vittrant, G. Zinc Oxide Nanowire-Parylene Nanocomposite Based Stretchable Piezoelectric Nanogenerators for Self-Powered Wearable Electronics. *J. Phys. Conf. Ser.* **2018**, *1052*, 012028. [CrossRef]
24. Jamond, N.; Chrétien, P.; Houzé, F.; Lu, L.; Largeau, L.; Maugain, O.; Travers, L.; Harmand, J.C.; Glas, F.; Lefeuvre, E.; et al. Piezo-Generator Integrating a Vertical Array of GaN Nanowires. *Nanotechnology* **2016**, *27*, 325403. [CrossRef] [PubMed]
25. Minary-Jolandan, M.; Bernal, R.A.; Kuljanishvili, I.; Parpoil, V.; Espinosa, H.D. Individual GaN Nanowires Exhibit Strong Piezoelectricity in 3D. *Nano Lett.* **2012**, *12*, 970–976. [CrossRef] [PubMed]
26. Agrawal, R.; Espinosa, H.D. Giant Piezoelectric Size Effects in Zinc Oxide and Gallium Nitride Nanowires. A First Principles Investigation. *Nano Lett.* **2011**, *11*, 786–790. [CrossRef] [PubMed]
27. Zhao, M.-H.; Wang, Z.-L.; Mao, S.X. Piezoelectric Characterization of Individual Zinc Oxide Nanobelt Probed by Piezoresponse Force Microscope. *Nano Lett.* **2004**, *4*, 587–590. [CrossRef]
28. Jamond, N.; Chrétien, P.; Gatilova, L.; Galopin, E.; Travers, L.; Harmand, J.-C.; Glas, F.; Houzé, F.; Gogneau, N. Energy Harvesting Efficiency in GaN Nanowire-Based Nanogenerators: The Critical Influence of the Schottky Nanocontact. *Nanoscale* **2017**, *9*, 4610–4619. [CrossRef] [PubMed]
29. Van de Walle, C.G.; Segev, D. Microscopic Origins of Surface States on Nitride Surfaces. *J. Appl. Phys.* **2007**, *101*, 081704. [CrossRef]
30. Donatini, F.; de Luna Bugallo, A.; Tchoulfian, P.; Chicot, G.; Sartel, C.; Sallet, V.; Pernot, J. Comparison of Three E-Beam Techniques for Electric Field Imaging and Carrier Diffusion Length Measurement on the Same Nanowires. *Nano Lett.* **2016**, *16*, 2938–2944. [CrossRef]

31. Zhernokletov, D.M.; Negara, M.A.; Long, R.D.; Aloni, S.; Nordlund, D.; McIntyre, P.C. Interface Trap Density Reduction for Al_2O_3/GaN (0001) Interfaces by Oxidizing Surface Preparation Prior to Atomic Layer Deposition. *ACS Appl. Mater. Interfaces* **2015**, *7*, 12774–12780. [CrossRef] [PubMed]
32. Siva Pratap Reddy, M.; Im, K.-S.; Lee, J.-H.; Caulmione, R.; Cristoloveanu, S. Trap and 1/f-Noise Effects at the Surface and Core of GaN Nanowire Gate-All-around FET Structure. *Nano Res.* **2019**, *12*, 809–814. [CrossRef]
33. Lüth, H. *Solid Surfaces, Interfaces and Thin Films*; Springer International Publishing: Cham, Switzerland, 2015; ISBN 978-3-319-10755-4.
34. Polenta, L.; Rossi, M.; Cavallini, A.; Calarco, R.; Marso, M.; Meijers, R.; Richter, T.; Stoica, T.; Lüth, H. Investigation on Localized States in GaN Nanowires. *ACS Nano* **2008**, *2*, 287–292. [CrossRef] [PubMed]
35. Zhang, Z.; Yates, J.T., Jr. Band Bending in Semiconductors: Chemical and Physical Consequences at Surfaces and Interfaces. *Chem. Rev.* **2012**, *112*, 5520–5551. [CrossRef] [PubMed]
36. King, P.D.C.; Veal, T.D.; Payne, D.J.; Bourlange, A.; Egdell, R.G.; McConville, C.F. Surface electron accumulation and the charge neutrality level in In_2O_3. *Phys. Rev. Lett.* **2008**, *101*, 116808. [CrossRef] [PubMed]
37. Bodecker, H.V.; Hornig, G. Link Invariants of Electromagnetic Fields. *Phys. Rev. Lett.* **2004**, *92*, 30406. [CrossRef] [PubMed]
38. Noguchi, M.; Hirakawa, K.; Ikoma, T. Intrinsic Electron Accumulation Layers on Reconstructed Clean InAs(100) Surfaces. *Phys. Rev. Lett.* **1991**, *66*, 2243–2246. [CrossRef] [PubMed]
39. Calarco, R.; Stoica, T.; Brandt, O.; Geelhaar, L. Surface-Induced Effects in GaN Nanowires. *J. Mater. Res.* **2011**, *26*, 2157–2168. [CrossRef]
40. Lopez Garcia, A.J.L.; Mouis, M.; Consonni, V.; Ardila, G. Dimensional Roadmap for Maximizing the Piezoelectrical Response of ZnO Nanowire-Based Transducers: Impact of Growth Method. *Nanomaterials* **2021**, *11*, 941. [CrossRef]
41. Park, C.H.; Chadi, D.J. Stability of Deep Donor and Acceptor Centers in GaN, AlN, and BN. *Phys. Rev. B* **1997**, *55*, 12995–13001. [CrossRef]
42. Qiu, C.H.; Pankove, J.I. Deep Levels and Persistent Photoconductivity in GaN Thin Films. *Appl. Phys. Lett.* **1997**, *70*, 1983–1985. [CrossRef]
43. Lin, T.Y.; Yang, H.C.; Chen, Y.F. Optical Quenching of the Photoconductivity in N-Type GaN. *J. Appl. Phys.* **2000**, *87*, 3404–3408. [CrossRef]
44. Kresse, G.; Dulub, O.; Diebold, U. Competing Stabilization Mechanism for the Polar ZnO(0001)-Zn Surface. *Phys. Rev. B* **2003**, *68*, 245409. [CrossRef]
45. Son, J.; Chobpattana, V.; McSkimming, B.M.; Stemmer, S. In-Situ Nitrogen Plasma Passivation of Al_2O_3/GaN Interface States. *J. Vac. Sci. Technol. A Vac. Surf. Film.* **2015**, *33*, 020602. [CrossRef]
46. Soudi, A.; Hsu, C.-H.; Gu, Y. Diameter-Dependent Surface Photovoltage and Surface State Density in Single Semiconductor Nanowires. *Nano Lett.* **2012**, *12*, 5111–5116. [CrossRef] [PubMed]
47. Xue, X.; Nie, Y.; He, B.; Xing, L.; Zhang, Y.; Wang, Z.L. Surface Free-Carrier Screening Effect on the Output of a ZnO Nanowire Nanogenerator and Its Potential as a Self-Powered Active Gas Sensor. *Nanotechnology* **2013**, *24*, 225501. [CrossRef] [PubMed]
48. Wang, C.-H.; Liao, W.-S.; Lin, Z.-H.; Ku, N.-J.; Li, Y.-C.; Chen, Y.-C.; Wang, Z.-L.; Liu, C.-P. Optimization of the Output Efficiency of GaN Nanowire Piezoelectric Nanogenerators by Tuning the Free Carrier Concentration. *Adv. Energy Mater.* **2014**, *4*, 1400392. [CrossRef]
49. Tao, R.; Mouis, M.; Ardila, G. Unveiling the Influence of Surface Fermi Level Pinning on the Piezoelectric Response of Semiconducting Nanowires. *Adv. Electron. Mater.* **2018**, *4*, 1700299. [CrossRef]
50. Liu, J.; Fei, P.; Song, J.; Wang, X.; Lao, C.; Tummala, R.; Wang, Z.L. Carrier Density and Schottky Barrier on the Performance of DC Nanogenerator. *Nano Lett.* **2008**, *8*, 328–332. [CrossRef]
51. Hinchet, R.; Lee, S.; Ardila, G.; Montès, L.; Mouis, M.; Wang, Z.L. Performance Optimization of Vertical Nanowire-Based Piezoelectric Nanogenerators. *Adv. Funct. Mater.* **2014**, *24*, 971–977. [CrossRef]
52. Sohn, J.I.; Cha, S.N.; Song, B.G.; Lee, S.; Kim, S.M.; Ku, J.; Kim, H.J.; Park, Y.J.; Choi, B.L.; Wang, Z.L.; et al. Engineering of Efficiency Limiting Free Carriers and an Interfacial Energy Barrier for an Enhancing Piezoelectric Generation. *Energy Environ. Sci.* **2013**, *6*, 97–104. [CrossRef]
53. Gao, J.; Zhang, X.; Sun, Y.; Zhao, Q.; Yu, D. Compensation Mechanism in N-Doped ZnO Nanowires. *Nanotechnology* **2010**, *21*, 245703. [CrossRef] [PubMed]
54. Lee, K.Y.; Bae, J.; Kim, S.; Lee, J.-H.; Yoon, G.C.; Gupta, M.K.; Kim, S.; Kim, H.; Park, J.; Kim, S.-W. Depletion Width Engineering via Surface Modification for High Performance Semiconducting Piezoelectric Nanogenerators. *Nano Energy* **2014**, *8*, 165–173. [CrossRef]
55. Hu, Y.; Lin, L.; Zhang, Y.; Wang, Z.L. Replacing a Battery by a Nanogenerator with 20 V Output. *Adv. Mater.* **2012**, *24*, 110–114. [CrossRef] [PubMed]
56. Xu, S.; Xu, C.; Liu, Y.; Hu, Y.; Yang, R.; Yang, Q.; Ryou, J.-H.; Kim, H.J.; Lochner, Z.; Choi, S.; et al. Ordered Nanowire Array Blue/Near-UV Light Emitting Diodes. *Adv. Mater.* **2010**, *22*, 4749–4753. [CrossRef] [PubMed]
57. Garcia, A.J.L.; Jalabert, T.; Pusty, M.; Defoor, V.; Mescot, X.; Montanino, M.; Sico, G.; Loffredo, F.; Villani, F.; Nenna, G.; et al. Size and Semiconducting Effects on the Piezoelectric Performances of ZnO Nanowires Grown onto Gravure-Printed Seed Layers on Flexible Substrates. *Nanoenergy Adv.* **2022**, *2*, 197–209. [CrossRef]

58. Gogneau, N.; Chrétien, P.; Sodhi, T.; Couraud, L.; Leroy, L.; Travers, L.; Harmand, J.-C.; Julien, F.H.; Tchernycheva, M.; Houzé, F. Electromechanical Conversion Efficiency of GaN NWs: Critical Influence of the NW Stiffness, the Schottky Nano-Contact and the Surface Charge Effects. *Nanoscale* **2022**, *14*, 4965–4976. [CrossRef]
59. Lu, S.; Liao, Q.; Qi, J.; Liu, S.; Liu, Y.; Liang, Q.; Zhang, G.; Zhang, Y. The Enhanced Performance of Piezoelectric Nanogenerator via Suppressing Screening Effect with Au Particles/ZnO Nanoarrays Schottky Junction. *Nano Res.* **2016**, *9*, 372–379. [CrossRef]
60. Largeau, L.; Galopin, E.; Gogneau, N.; Travers, L.; Glas, F.; Harmand, J.-C. N-Polar GaN Nanowires Seeded by Al Droplets on Si(111). *Cryst. Growth Des.* **2012**, *12*, 2724–2729. [CrossRef]
61. Brubaker, M.D.; Levin, I.; Davydov, A.V.; Rourke, D.M.; Sanford, N.A.; Bright, V.M.; Bertness, K.A. Effect of AlN Buffer Layer Properties on the Morphology and Polarity of GaN Nanowires Grown by Molecular Beam Epitaxy. *J. Appl. Phys.* **2011**, *110*, 053506. [CrossRef]
62. Bertness, K.A.; Roshko, A.; Mansfield, L.M.; Harvey, T.E.; Sanford, N.A. Nucleation Conditions for Catalyst-Free GaN Nanowires. *J. Cryst. Growth* **2007**, *300*, 94–99. [CrossRef]
63. Largeau, L.; Dheeraj, D.L.; Tchernycheva, M.; Cirlin, G.E.; Harmand, J.C. Facet and In-Plane Crystallographic Orientations of GaN Nanowires Grown on Si(111). *Nanotechnology* **2008**, *19*, 155704. [CrossRef]
64. Songmuang, R.; Landré, O.; Daudin, B. From Nucleation to Growth of Catalyst-Free GaN Nanowires on Thin AlN Buffer Layer. *Appl. Phys. Lett.* **2007**, *91*, 251902. [CrossRef]
65. Jacopin, G.; De Luna Bugallo, A.; Rigutti, L.; Lavenus, P.; Julien, F.H.; Lin, Y.-T.; Tu, L.-W.; Tchernycheva, M. Interplay of the Photovoltaic and Photoconductive Operation Modes in Visible-Blind Photodetectors Based on Axial p-i-n Junction GaN Nanowires. *Appl. Phys. Lett.* **2014**, *104*, 023116. [CrossRef]
66. Massalski, T.B. *Binary Alloy Phase Diagrams*; ASM International: Almere, The Netherlands, 1986; Volume 2, pp. 164–165.
67. Saleem, U.; Birowosuto, M.D.; Gogneau, N.; Coquet, P.; Tchernycheva, M.; Wang, H. Yellow and Green Luminescence in Single-Crystal Ge-Catalyzed GaN Nanowires Grown by Low Pressure Chemical Vapor Deposition. *Opt. Mater. Express* **2017**, *7*, 1995–2004. [CrossRef]
68. Le Formal, F.; Tétreault, N.; Cornuz, M.; Moehl, T.; Grätzel, M.; Sivula, K. Passivating Surface States on Water Splitting Hematite Photoanodes with Alumina Overlayers. *Chem. Sci.* **2011**, *2*, 737–743. [CrossRef]
69. Kim, H.; Bae, H.; Bang, S.W.; Kim, S.; Lee, S.H.; Ryu, S.-W.; Ha, J.-S. Enhanced Photoelectrochemical Stability of GaN Photoelectrodes by Al2O3 Surface Passivation Layer. *Opt. Express* **2019**, *27*, A206–A215. [CrossRef] [PubMed]
70. Ek, A.; Reichel, C.; Richter, A.; Benick, J. Influence of Layer Thickness on Passivation Properties in SiO_x/Al_2O_3 Stacks. *J. Appl. Phys.* **2020**, *127*, 235303. [CrossRef]
71. Simon, D.K.; Jordan, P.M.; Mikolajick, T.; Dirnstorfer, I. On the Control of the Fixed Charge Densities in Al_2O_3-Based Silicon Surface Passivation Schemes. *ACS Appl. Mater. Interfaces* **2015**, *7*, 28215–28222. [CrossRef]
72. Ghods, A.; Zhou, C.; Ferguson, I.T. Enhancement in Electrical and Optical Properties of Field-Effect Passivated GaN Blue Light Emitting Diodes. *Semicond. Sci. Technol.* **2021**, *36*, 115018. [CrossRef]
73. Seo, M.A.; Yoo, J.; Dayeh, S.A.; Picraux, S.T.; Taylor, A.J.; Prasankumar, R.P. Mapping Carrier Diffusion in Single Silicon Core–Shell Nanowires with Ultrafast Optical Microscopy. *Nano Lett.* **2012**, *12*, 6334–6338. [CrossRef] [PubMed]
74. Schneegans, O.; Chretien, P.; Houze, F. Apparatus for Measuring the Local Electrical Resistance of a Surface. French patent, FR 1001940, 2010International PCT, WO2011/138738, 2011. U.S. Patent 9594101 B2, 2017.
75. Levinshtein, M.E.; Rumyantsev, S.L.; Shur, M.S. (Eds.) *Properties of Advanced Semiconductor Materials: GaN, AlN, InN, BN, SiC, SiGe*; Wiley: New York, NY, USA, 2001; p. 1.
76. Gogneau, N.; Chrétien, P.; Galopin, E.; Guilet, S.; Travers, L.; Harmand, J.-C.; Houzé, F. Impact of the GaN Nanowire Polarity on Energy Harvesting. *Appl. Phys. Lett.* **2014**, *104*, 213105. [CrossRef]
77. Liu, M.; Sun, J.; Chen, Q. Influences of Heating Temperature on Mechanical Properties of Polydimethylsiloxane. *Sens. Actuators A Phys.* **2009**, *151*, 42–45. [CrossRef]
78. Pérez-García, B.; Zúñiga-Pérez, J.; Muñoz-Sanjosé, V.; Colchero, J.; Palacios-Lidón, E. Formation and Rupture of Schottky Nanocontacts on ZnO Nanocolumns. *Nano Lett.* **2007**, *7*, 1505–1511. [CrossRef] [PubMed]

Disclaimer/Publisher's Note: The statements, opinions and data contained in all publications are solely those of the individual author(s) and contributor(s) and not of MDPI and/or the editor(s). MDPI and/or the editor(s) disclaim responsibility for any injury to people or property resulting from any ideas, methods, instructions or products referred to in the content.